Article published online: 2021-07-22

Applications of dual energy CT in clinical practice: A pictorial essay

Parang S Sanghavi, Bhavin G Jankharia
Jankharia Imaging Centre, Mumbai, Maharashtra, India

Correspondence: Dr. Parang S Sanghavi, B - 4/402, Building No 7, Ravikiran, Tilak Nagar (West), Mumbai - 400 089, Maharashtra, India.
E-mail: sanghaviparang@gmail.com

Abstract

In dual-energy CT (DECT), two different x-ray spectra are used to acquire two image datasets of the same region, to allow the analysis of energy-dependent changes in the attenuation of different materials. Each type of material demonstrates a relatively specific change in attenuation between images obtained with a high-energy spectrum and those obtained with a low-energy spectrum. Based on the relatively specific change in attenuation with two different energies, material composition information can be obtained to allow tissue characterization. The DECT ability of material differentiation allows bone removal in various CT angiography studies and bone marrow edema depiction, while with material optimization, metal artefacts can be significantly reduced to almost nil. DECT allows material separation to differentiate uric acid crystals from calcium to determine the composition of urinary calculi and to diagnose gout. Using the DECT ability of material decomposition, iodine maps can be generated, which are useful in the evaluation of any enhancing lesion in the body without the need to obtain a plain scan and allow perfusion maps to be created in cases of pulmonary thromboembolism.

Key words: Dual energy CT; iodine map; material; metal artefact; uric acid

Introduction

In diagnostic imaging, the photoelectric effect is the most important mechanism by which the x-ray photons interact with matter. The chances of this effect increase as the energy of the x-ray beam approaches the K_{edge} of the particular atom.[1] Different atoms have different K_{edge} values and hence behave differently at different energies of the x-ray beam.

In dual-energy CT, two different x-ray spectra are used to acquire two image datasets of the same anatomic region, allowing analysis of energy dependent changes in the attenuation of different materials.[2] Every material shows a relatively specific change in attenuation between images obtained with a high and a low-energy spectrum and this attenuation difference allows better characterization of the tissues. Two different materials that show similar attenuation on images acquired with one of the two energy spectra, may show substantial differences in their attenuation on the images acquired with the other spectrum and hence may be easily differentiated.[3]

There are multiple techniques available for dual energy CT imaging which can be broadly classified as:
1) Dual source DECT
2) Single source DECT.

Access this article online	
Quick Response Code:	Website: www.ijri.org
	DOI: 10.4103/ijri.IJRI_241_19

Cite this article as: Sanghavi PS, Jankharia BG. Applications of dual energy CT in clinical practice: A pictorial essay. Indian J Radiol Imaging 2019;29:289-98.

Received: 03-Jun-2019 **Revision:** 15-Sep-2019
Accepted: 08-Oct-2019 **Published:** 30-Oct-2019

Single source DECT can be further divided based on the exact mechanism to generate two different energy spectra as:

1) Fast kV switching
2) Dual layer detector
3) Slow kV switching
4) Dual spiral dual energy
5) Twin beam dual energy.

We use the Siemens Somatom Definition Edge CT scanner which is based upon a single source twin beam dual energy technique [Figure 1].

In twin beam DECT, two different filters Tin [Sn] and Gold [Au] are used to split the x-ray beam from a single source into two beams of different energies. The greatest advantage of this technique over the many of the other techniques mentioned above is eliminating temporal mis-registration.

Applications in Clinical Practice

Material differentiation

Bone removal in angiography

As DECT has the ability to differentiate different materials from one another, calcium in the bones is readily separated from iodine in the contrast media. Hence the bones in any angiography study can be easily removed. This is particularly useful in cerebral [Figure 2] and lower limb angiography [Figures 3 and 4], where manual methods can be difficult and time consuming, especially when the vessels lie close to bones.[4,5] Similarly, calcified plaques can be removed for better visualisation of the lumen [Figure 5].

Bone marrow edema

Bone marrow edema is best visualised on MRI imaging. However with DECT, it is now possible to evaluate bone marrow edema on CT scan as well. As DECT can differentiate calcium from other elements, it can also selectively remove calcium from the region of interest. This is called virtual non-calcium (VNC) technique and it allows visualisation of bone marrow edema.[6] Multiple studies have validated this technique for bone marrow edema detection.[7,8]

It is especially useful in acute fractures where MRI may not be possible [Figures 6 and 7]. Kaup M *et al*.[9] demonstrated the utility of DECT for bone marrow edema evaluation in osteoporotic vertebral compression fractures and found that its diagnostic performance approached that of MRI.

Material optimisation

Metal artefact reduction

Metal in prosthesis can cause significant artefacts and hamper evaluation of periprosthetic soft tissue. These metal artefacts are caused by beam hardening artefacts.[10]

Radiographs are typically obtained post-operatively but they have low sensitivity and specificity.[11] MRI is a great tool to assess bone marrow edema and soft tissue lesions but the images are distorted by metal artefacts.[12]

With the conventional CT, multiple techniques are available to reduce the metal artefacts.[13] Increasing in tube current, increasing voltage and reducing slice thickness can help reduce metal artefacts. Various modifications in reconstructions techniques like changing the deconvolution

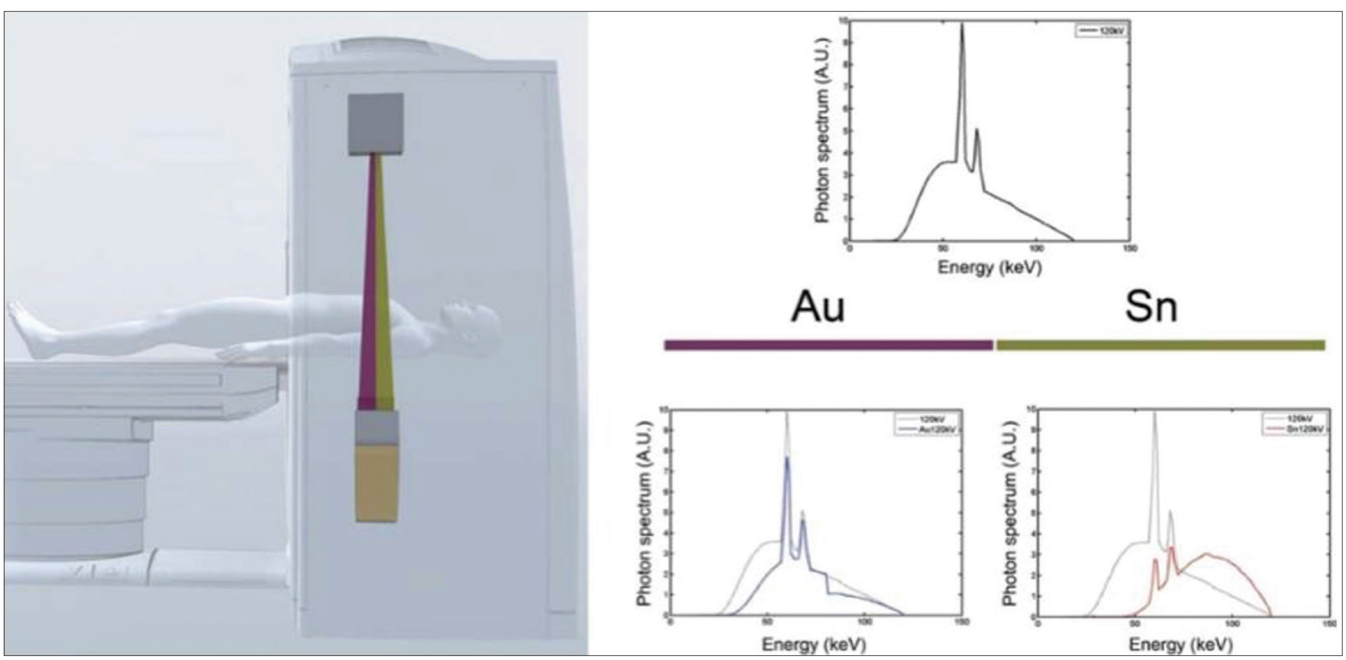

Figure 1: In twin beam DECT, two different filters Tin (Sn) and Gold (Au) are used to split the x-ray beam into two beams of different energies. The Gold (Au) filter, filters the high energy photons and produces a low energy beam while Tin (Sn) filter, filters the low energy photons and produces a high energy beam

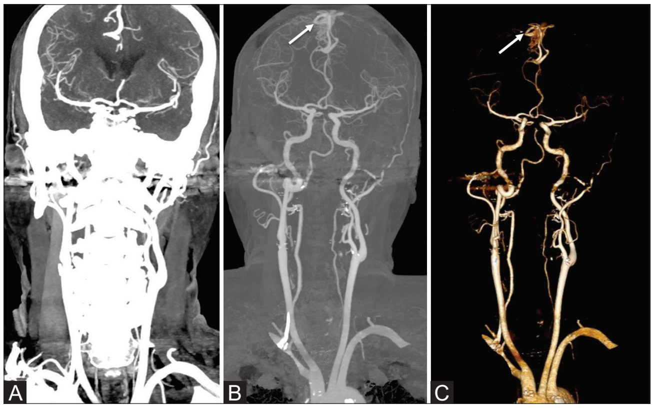

Figure 2 (A-C): A routine cerebral CT angiography study (A) shows carotid and cerebral arteries overlapped by bones making it difficult to visualise them. With DECT bone removal tool, all the bones are effectively and selectively removed allowing clear visualisation of the arteries with AVM (arrow) as shown in this MIP image (B). Similarly the arteries with AVM (arrow) can also be evaluated in VRT image (C) with bone removal

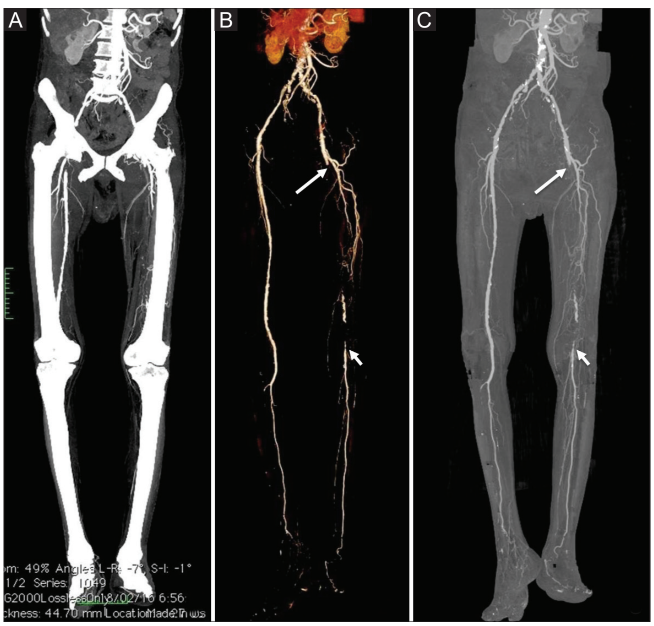

Figure 4 (A-C): A lower limb CT angiography study (A) shows arteries overlap by bones. DECT bone removal technique VRT (B) and MIP (C) images shows the occlusion of the left superficial femoral artery (arrow) well with extensive collateral circulation and distal reformation of the popliteal and the tibial arteries (short arrow)

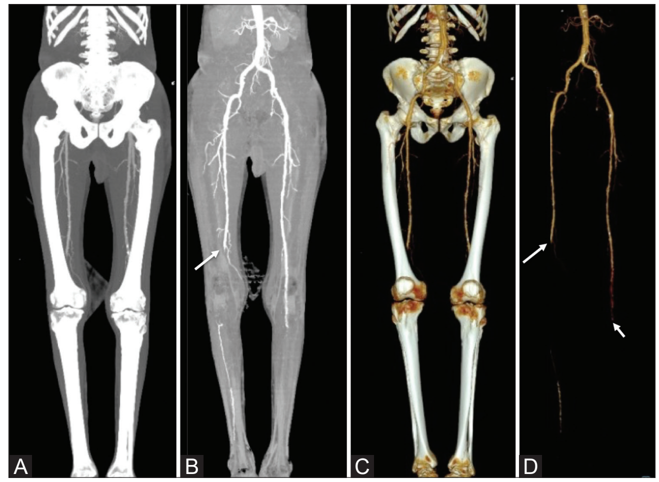

Figure 3 (A-D): A routine lower limb CT angiography study (A) shows arteries overlapped by the long bones. With DECT bone removal technique in MIP image (B), the right popliteal artery occlusion (arrow) is clearly visualised with distal reformation of the tibial artery seen via collateral circulation. Similarly left distal popliteal artery occlusion (short arrow) just at the level of its division is also seen. Similarly VRT images without (C) and with (D) bone removal also shows the pathologies (arrows) well

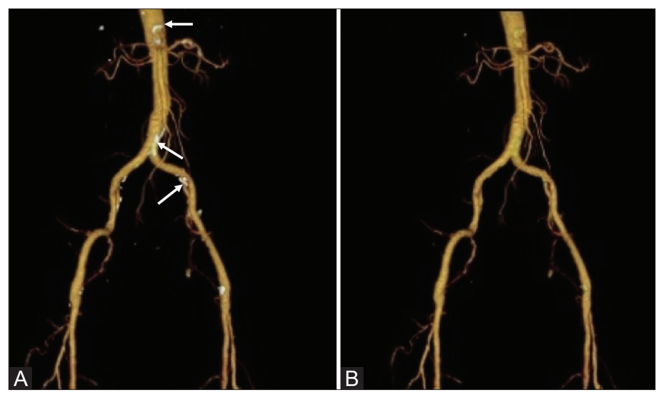

Figure 5 (A and B): Same case as shown in Figure 4, also shows diffuse atherosclerotic wall calcification (arrows), compromising accurate lumen visualisation (A). With DECT calcium removal technique applied on VRT images (B) the calcium in the wall of the arteries is effectively removed, allowing the visualisation of the underlying lumen easily

kernel from bone to soft tissue or smooth kernel, using interactive reconstructions and extending the Hounsfield unit scale from 4000 to 40000 HU can also help reduce metal artefacts.

Using DECT, the artefacts from metal can be significantly reduced to almost nil. As the artefacts are more at lower energy x-ray beams, the monochromatic images at higher keV settings show significantly less artefacts.

Additionally, iterative reconstruction protocols such as iMAR (interactive metal artefact reduction) can be used that further reduce the metal artefacts. When both the techniques are used together, the final result shows almost nil metal artefacts [Figures 8 and 9]. This allows the visualisation of periprosthetic soft tissue to identify complications such as periprosthetic osteolyis, fracture, infection, aseptic loosening, focal particle disease and tumor. Metal artefact reduction can also be used for evaluation of stents and to detect endoleak after aneurysm repair.[14]

Material separation

DECT has the ability to separate different materials based on their specific dual energy ratio. Hence, uric acid crystal can be separated from calcium, both of which otherwise appears hyperdense on conventional single energy CT.

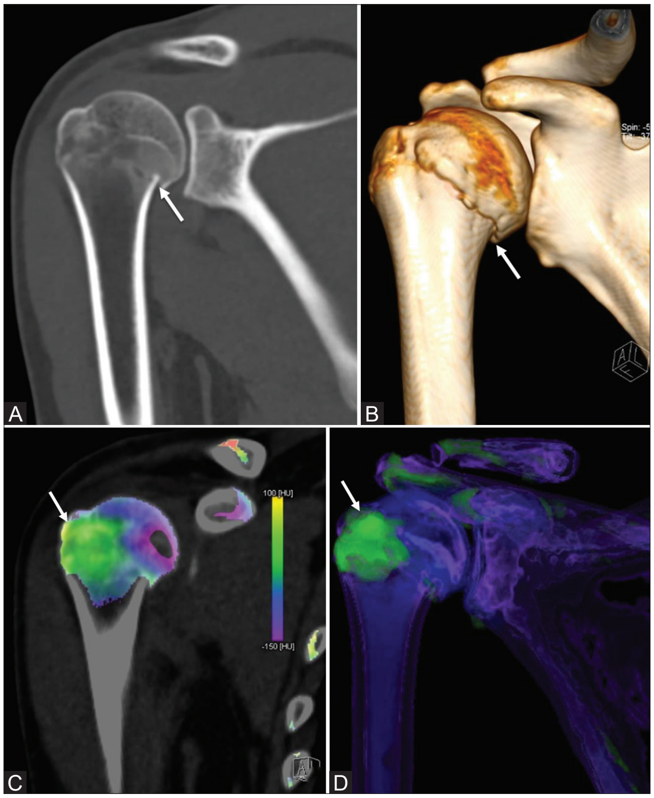

Figure 6 (A-D): CT image in coronal reconstruction (A) and 3D reconstruction (B) shows fractures (arrows) involving the neck and the greater tuberosity of the right humerus. With DECT, the bone marrow edema (arrows) can be seen in the the neck and the greater tuberosity of the humerus as seen in DECT coronal reconstruction (C) and DECT 3D reconstruction (D)

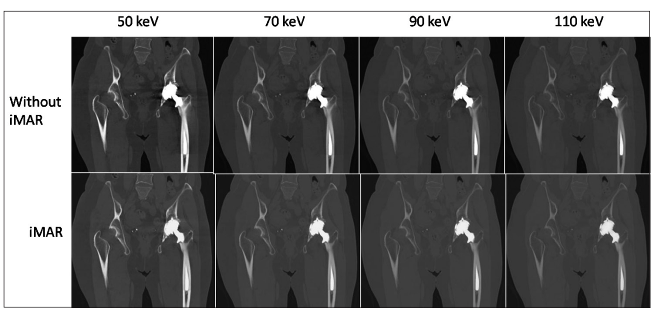

Figure 8: In a known case of left total hip replacement, the conventional CT images shows extensive metal artefacts, compromising adequate visualisation of the bones and the soft tissue. With DECT, multiple reconstructions at various keV can be obtained and with progressively increasing keV, the metal artefacts keep reducing. Addition of iterative reconstruction (iMAR), further reduces metal artefacts and when both techniques are combined, the final image shows almost nil artefacts, allowing accurate evaluation of the bone and the soft tissue

Urinary stones

As different types of renal calculi are treated differently, knowledge of the composition of stones may guide management decisions and predict the effectiveness of therapy. For example, uric acid calculi can be managed medically with urine alkalinization that facilitates dissolution, while non-uric acid calculi need other lines of treatment such as lithotripsy or surgery.[15]

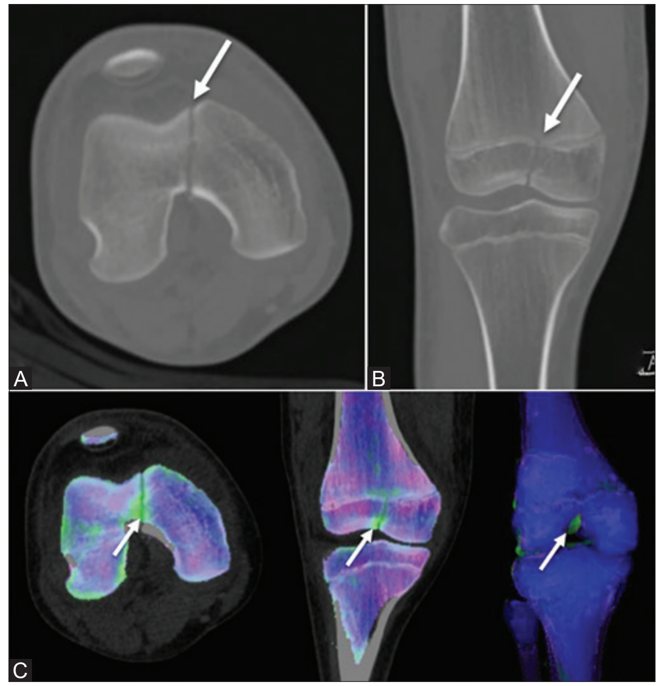

Figure 7 (A-C): Another example of bone marrow edema seen with DECT, in a case of trauma to the right knee, 1 week ago. CT scan in axial (A) and coronal (B) reconstructions shows a linear undisplaced fracture (arrows) in the distal femur in the intercondylar region. DECT images (C) also shows mild residual edema (arrows) at the fracture site

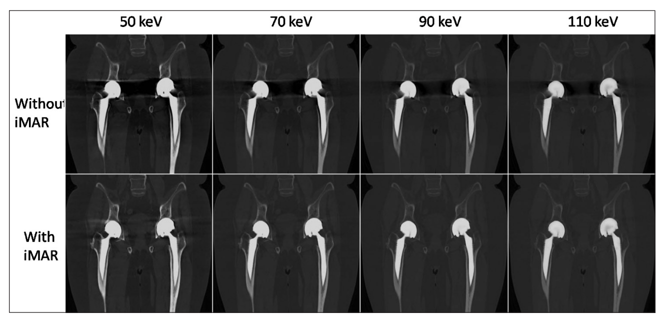

Figure 9: Another example of metal artefact reduction in a patient with bilateral total hip replacement. Higher keV images shows less metal artefacts and addition of iterative reconstruction (iMAR) further reduces the metal artefacts and when both techniques are combined, the final image shows almost nil artefacts

Using DECT, it is possible to differentiate uric acid from non-uric acid calculi. Keeping the dual energy ratio at 1.05, the uric acid stones lie below the line/slope and are coloured red, whereas the non-uric acid stones lie above the line/slope and are differently colour-coded (blue) [Figures 10 and 11].

Gout

Gout is characterized by an inflammatory response to the deposition of monosodium urate (MSU) crystals in the joints and soft tissue, which leads to acute or chronic arthropathy and gouty tophi formation. Diagnosis can be made on clinical and biochemical bases, and definite diagnosis requires microscopic demonstration of MSU crystals from

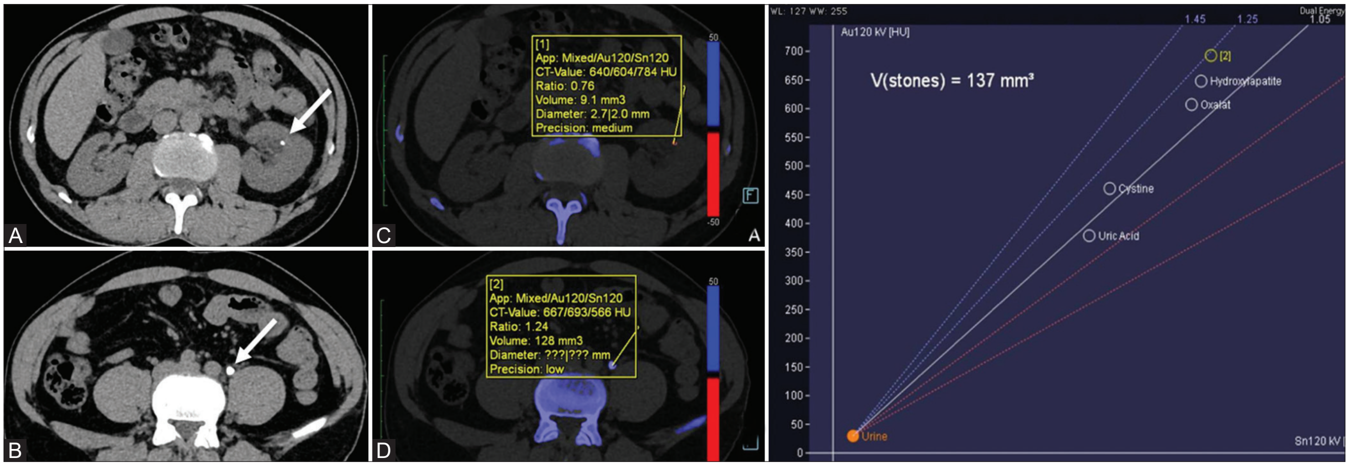

Figure 10 (A-D): The conventional CT images shows the calculi (arrows) in the kidney (A) and ureter (B) as hyperdense structures and their composition cannot be determined. With DECT uric acid calculus is shown in red (C) while non-uric acid calculus is shown as blue (D), allowing their differentiation. The graph also helps shows the two calculi differently, with the uric acid calculus lying below the line, and non-uric acid lying above

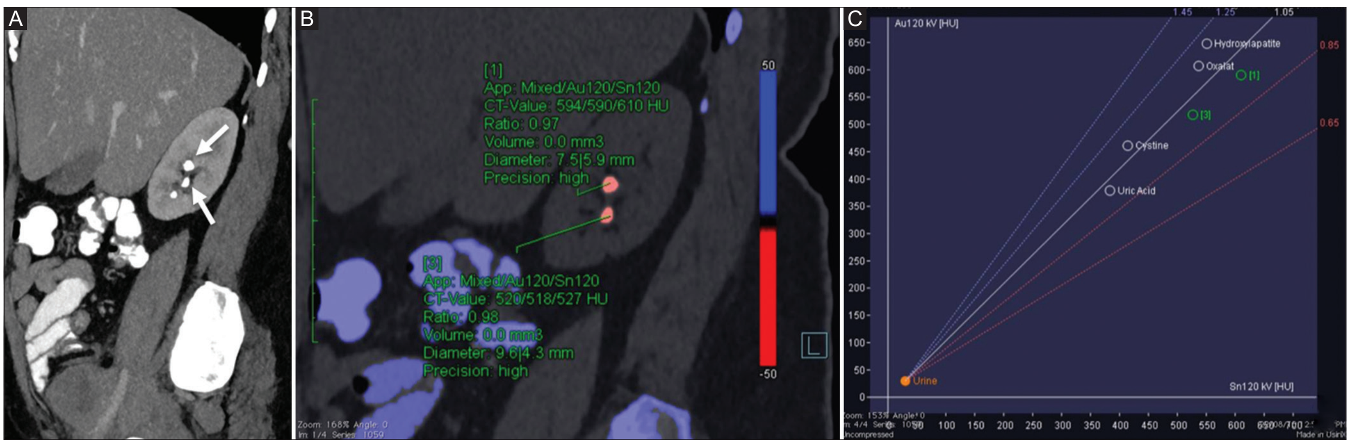

Figure 11 (A-C): Another example of urinary calculi (arrows), two calculi are seen in the kidney in the CT scan image (A). DECT the calculus red (B) in colour and falling below the line (C), thus confirming uric acid calculi

the aspiration of the joint fluid,[16] a method that is invasive and may have false negative results.

Keeping the dual energy ratio specific to uric acid crystals, the uric acid crystals are coloured green, whereas calcium is coloured blue. The diagnosis of gout can be easily made, non-invasively [Figure 12].

With DECT, it is also possible to quantify the overall tophus burden or volume of urate deposition without any user variability. Thus, makes DECT an ideal tool for evaluating any change in tophus burden and can be used for follow-up to document response to treatment[17] [Figure 13].

Material decomposition

Iodine maps

Lung

Pulmonary thromboembolism

The dual energy iodine maps allow us to evaluate lung perfusion and hence are useful to demonstrate perfusion defects in cases of pulmonary thromboembolism.

Figure 12 (A and B): A 35 years male presented with pain and swelling in right foot and wrist. Serum uric acid-13 mg/dl. Radiographs of both feet, knees and wrists (A) shows juxta-articular erosions (arrows) around right 1st metatarsophalangeal joint, right lateral femoral condyle, right distal ulna and 5th carpometacarpal joint with soft tissue. Diagnosis of gout was made. B. DECT (B) allows visualisation of the urate crystals seen as green coloured areas (arrows), confirming the diagnosis. Also, it shows involvement of the asymptomatic and radiographically occult areas and displays total tophus volume

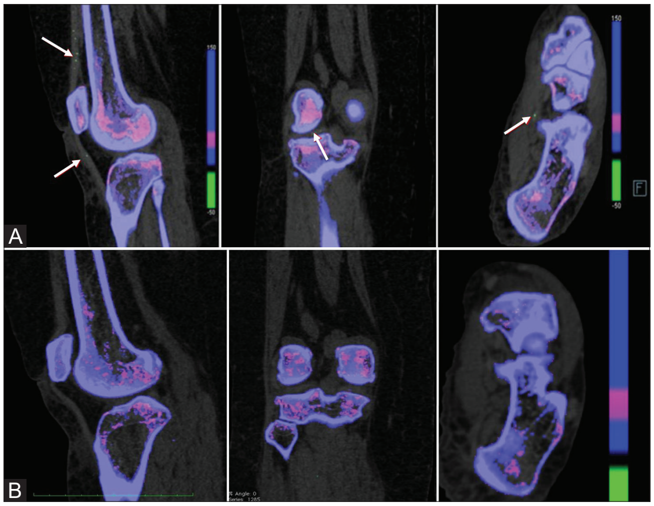

Figure 13 (A and B): A 38 years female presented with bilateral knee pain with normal serum uric acid levels. The DECT (A) showed small foci of urate crystal deposition (arrows) in both the knees and the left foot, confirming the diagnosis of gout and the patient was put on treatment with allopurinol. The follow up DECT scan (B) post 2 months of treatment shows significant improvement and resolution of the urate crystals, suggestive of response to treatment

Additionally, the dual energy iodine maps also improve visualisation of filling defects/thrombi in a small segmental or subsegmental artery. Fink *et al*.[18] showed the sensitivity and specificity of dual-energy CT perfusion mapping for the assessment of pulmonary embolism to be 100% on a per patient basis and 60-66.7% and 99.5-99.8% on a per segment basis, as compared to CT angiography.

In patients with pulmonary thromboembolism, the dual energy perfusion maps show peripheral wedge-shaped areas of reduced perfusion representing perfusion defects [Figure 14]. They are also very useful for the follow up of such patients who are treated with anticoagulants to demonstrate both a decrease in perfusion defects as well as the thrombi [Figures 15 and 16].

One should keep in mind the areas where artefacts are commonly seen and should not misinterpret them as areas of perfusion defects. These artefactual perfusion defects are commonly seen in the upper lobes due to beam hardening artefacts, in the medial segment of the right middle lobe and lingula due to cardiac pulsation and in the lung bases due to diaphragmatic motion. The other common pitfall is apparent perfusion defects in an area of lung parenchyma with systemic arterial supply. Also, parenchymal diseases such as collapse, consolidation, masses and emphysema show perfusion defects.[19]

Lung nodule

With DECT a single contrast enhanced scan is sufficient to differentiate an enhancing nodule from calcification with the use of virtual nonenhanced image reconstructions.[20] The enhancing and non-enhancing components of a heterogeneous lesion are better appreciated on iodine maps, which also help target the appropriate area for biopsy, to increase the yield [Figure 17].

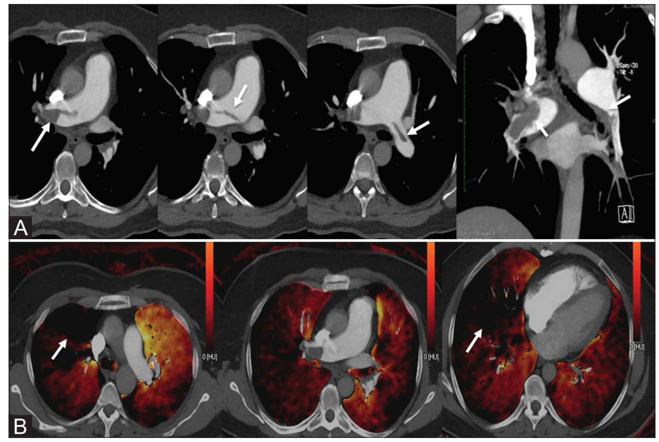

Figure 14 (A and B): CT Pulmonary angiography (A) shows a saddle thrombus (arrows) involving both the pulmonary arteries and also extending into the right upper and lower lobe branches. The DECT perfusion maps (B) shows patchy perfusion defects (arrows) in the right upper and lower lobes

Degree of contrast enhancement is an important factor to differentiate a benign from a malignant lesion.[21] Hence dual energy analysis with iodine maps is very useful in the evaluation of solitary or multiple pulmonary nodules. The enhancement in a nodule is not always easily appreciable on routine CT scan and DECT iodine maps help confirm or rule out enhancement conclusively [Figures 18 and 19].

Difference in the contrast wash out pattern of a metastatic nodule can be used to evaluate various types of primary malignant tumors. For example, metastases from colorectal carcinoma, malignant melanoma and thyroid carcinoma show a distinct wash out pattern whereas those from lung cancer, salivary gland cancer and sarcoma show increased enhancement in the delayed phase images.[22]

Liver lesions

A hypervascular lesion is more conspicuous on lower kV images on an arterial phase of the study, as iodine is more attenuating at lower energies.[23] DECT may be used to identify fat, iron, calcium, or hemorrhage within the tumor. Virtual non-enhanced images can be used to differentiate calcification in a lesion from enhancement.

DECT iodine maps are especially useful in differentiating a simple cyst from a complex cyst as they show the subtle enhancement in the lesion very well, which is often difficult to appreciate on a single energy CT scan [Figures 20 and 21].

Kidney lesions

DECT is useful in differentiating a hyperdense cyst from an enhancing solid tumor. A hyperdense cyst containing proteinaceous material or blood products may mimic a

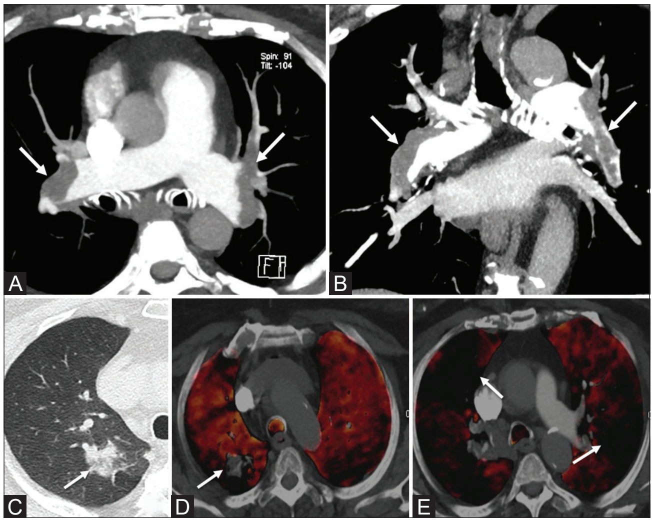

Figure 15 (A-E): CT Pulmonary angiography axial (A) and coronal (B) images shows extensive bilateral pulmonary thromboembolism (arrows). The HRCT axial (C) image shows a developing infarct (arrow) in the posterior segment of the right upper lobe. The DECT images (D and E) shows perfusion defects (arrows) in the lung parenchyma bilaterally with the infarct in the right upper lobe

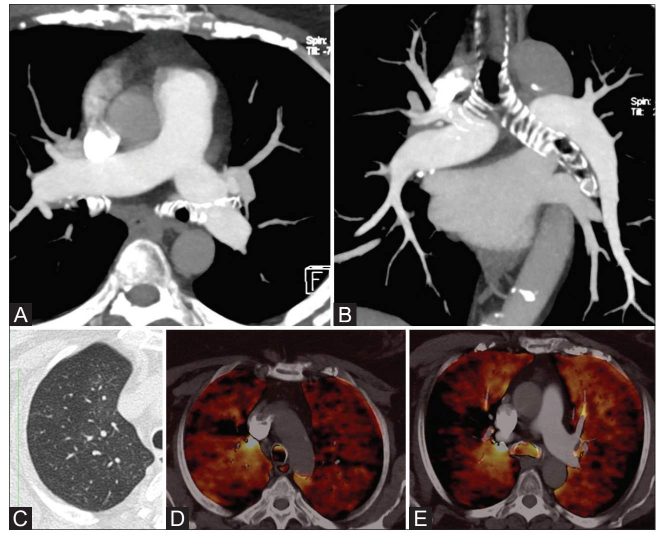

Figure 16 (A-E): The follow up CT Pulmonary angiography axial (A) and coronal (B) images, after 3 months of anticoagulation treatment shows complete resolution of the bilateral pulmonary thromboembolism. The HRCT axial (C) image shows resolution of the infarct in the right upper lobe. The DECT images (D and E) shows reversal of the perfusion defects in the lung parenchyma bilaterally

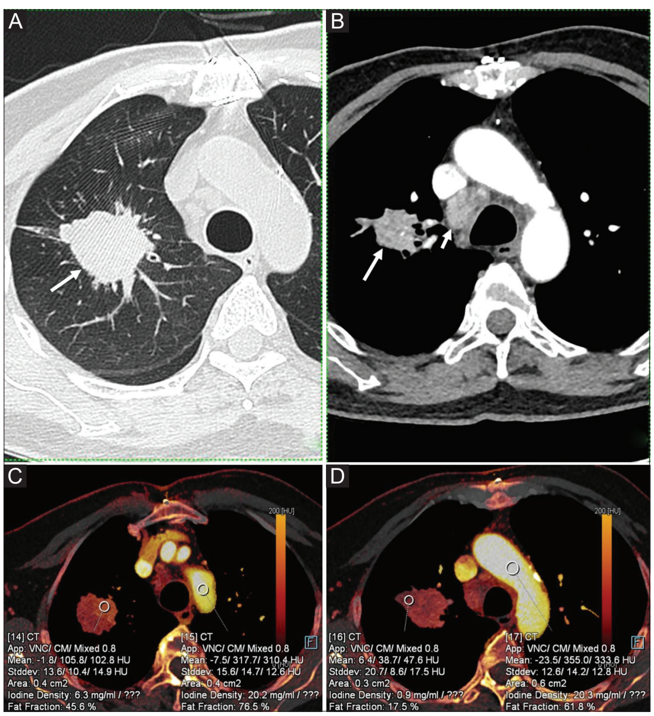

Figure 17 (A-D): The plain HRCT (A) and contrast (B) axial images shows an ill-defined spiculated enhancing mass (arrow) in the right upper lobe with mediastinal lymphadenopathy (short arrow). The DECT axial images shows the more enhancing part with higher iodine uptake in the medial part of the mass (C), which can be targeted for biopsy, while the lateral part (D) shows relatively less enhancement

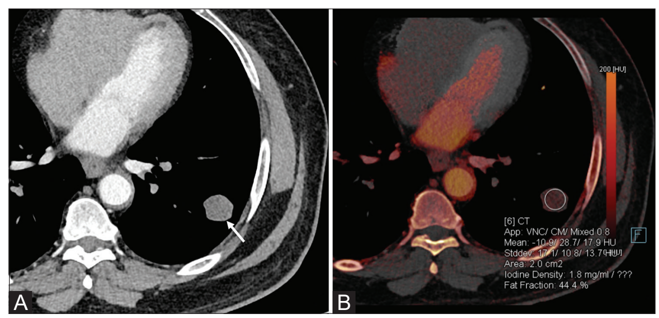

Figure 18 (A and B): The axial image (A) of the lungs shows a nodule (arrow) in the left lung with questionable enhancement. The DECT iodine map (B) help rule out enhancing nodule by showing no significant iodine uptake, hence suggestive of an old healed granuloma

solid enhancing tumor on a contrast enhanced scan. In such situations, iodine maps help as a hyperdense cyst will not show iodine uptake. Also, virtual non-enhanced images will show hyperdense contents in the cyst. Similarly, enhancement in a hyperdense lesion may be difficult to appreciate on routine CT images and DECT iodine maps show the enhancement well even in hyperdense parts of the lesion [Figure 22].

Adrenal lesions

The majority of the adrenal lesions seen on an abdomen CT scan are benign. On imaging the diagnosis of a benign adrenal lesion can be confidently made if it shows a Hounsfield value (HU) value of less than 10 on an unenhanced image (adenoma), shows macroscopic fat (myelolipoma) or has attenuation of water (cyst). The appearance of an adenoma on DECT is variable and may show decrease or increase in attenuation at lower kV images than higher, depending on the amount of lipid within the lesion.[24] DECT iodine maps can help pick up enhancing focal lesions in an adrenal gland [Figure 23].

Bowel pathologies

DECT is helpful in the evaluation of inflammatory bowel pathologies and shows the inflammation/enhancement of

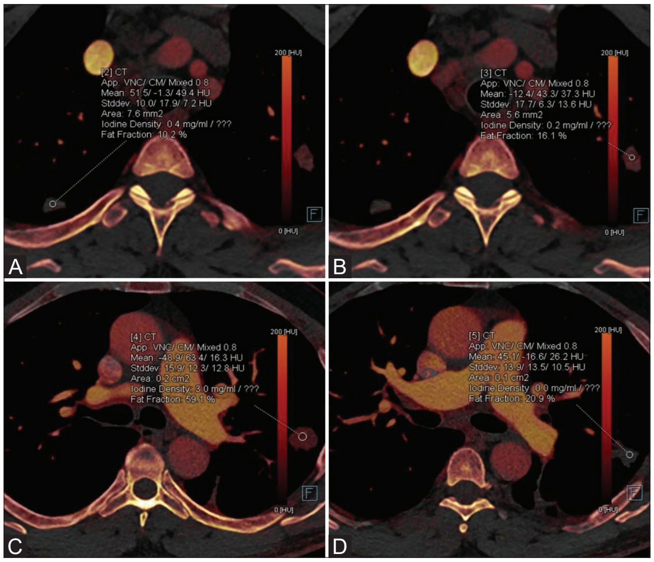

Figure 19 (A-D): DECT iodine maps (A, B and D) shows no significant iodine uptake in most of the nodules. Only one nodule (C) shows significant iodine uptake, worrisome for active nodule

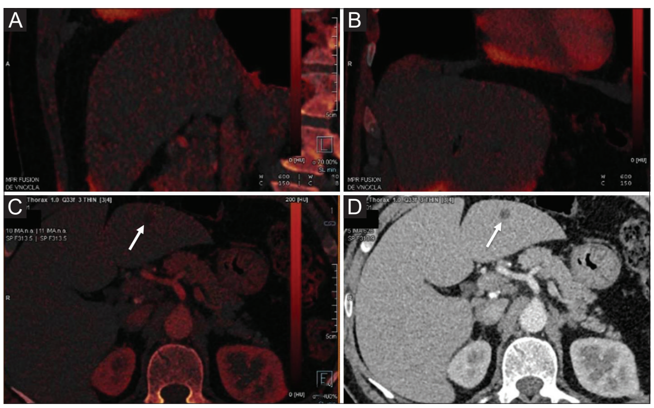

Figure 21 (A-D): The contrast enhanced abdomen image (D) shows a hypodense lesion (arrow) in the left lobe of the liver. The DECT iodine maps (A-C) shows no significant iodine uptake (arrow) suggestive of a simple cyst

the wall better [Figure 24]. It is also useful in assessing the severity and evaluate extraintestinal manifestations. Iodine maps demonstrate bowel wall enhancement/hyperemia in cases of inflammatory bowel disease. Coexisting neoplastic lesion can also be better assessed with DECT in such cases.

Post ablation analysis

Radiofrequency ablation (RFA) is now frequently used to treat a focal lesion in the liver, lung or kidney. It is important to detect residual tumor post RFA to decide if re-ablation is necessary. Conventionally, contrast enhanced single energy CT has been used to evaluate the success of RFA, and it may be difficult to pick up residual tumor and differentiate it from post ablation changes. DECT allows better depiction of the enhancing component in residual lesions using iodine overlay images, while the necrotic post-ablation regions appear avascular and do not show iodine uptake [Figure 25]. Monochromatic images also allow selection of the optimal

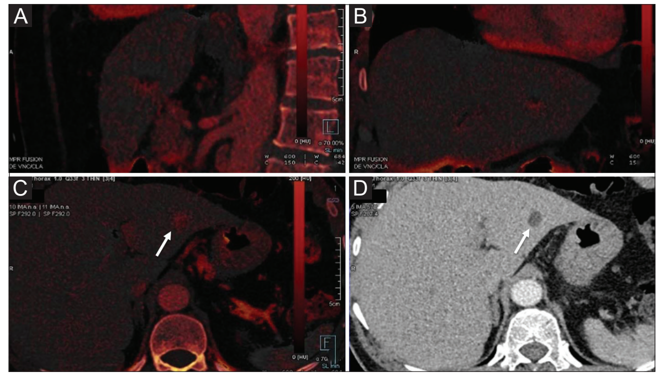

Figure 20 (A-D): A 53 years female, treated case of carcinoma breast, came for follow up scan. The contrast enhanced abdomen image (D) shows a hypodense lesion (arrow) in the left lobe of the liver. The DECT iodine maps (A-C) shows significant iodine uptake (arrow) suggestive of an enhancing lesion, worrisome for metastatic disease, which was later proved with biopsy

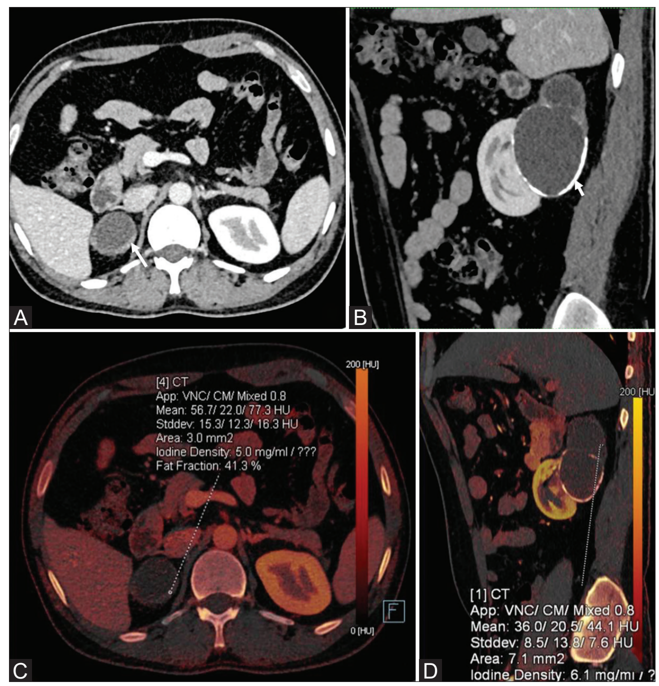

Figure 22 (A-D): The contrast enhanced CT shows a bilobed complex cystic lesion arising exophytically from the right kidney. The superior lobule shows thick walls with measurable enhancement (arrow) (A) while the inferior lobule shows wall calcification (short arrow) (B). The DECT iodine maps (C and D) shows definite iodine uptake in the thick walls of the superior lobule, suggestive of bosniak class 3 cystic lesion

keV that shows the best contrast to noise ratio between the tissues, thus allowing better evaluation of the interface between the ablation zone and surrounding tissue.[25]

Atomic number maps (Rho/Z)

The new dual energy CT application allows calculation of the atomic number in the lesion, for separation of various materials. Mileto *et al*.[26] showed that non-enhancing renal cysts, including hyperattenuating cysts, can be discriminated from enhancing masses on effective atomic number maps. They concluded 8.36 value was the optimal threshold with

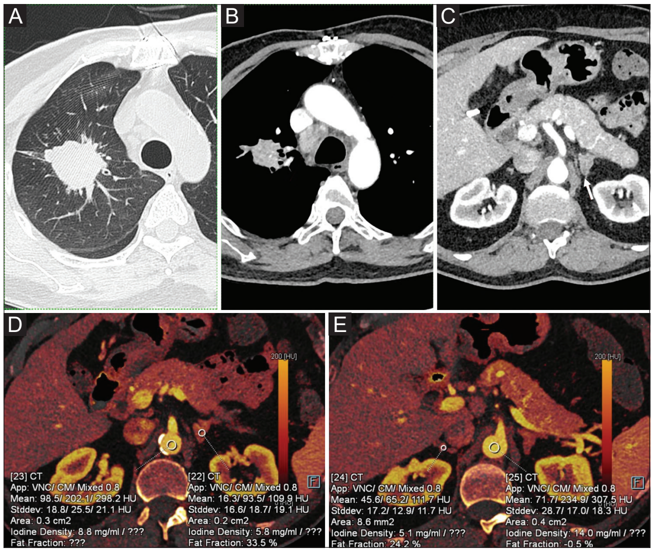

Figure 23 (A-E): The same case of carcinoma of lung (A and B) as shown in Figure 17, also shows an enhancing nodule in the left adrenal gland (arrow) (C), worrisome for metastatic disease. The DECT iodine maps confirms the iodine uptake in the left adrenal gland nodule (E), and also shows another nodule with iodine uptake in the right adrenal gland (D) as well

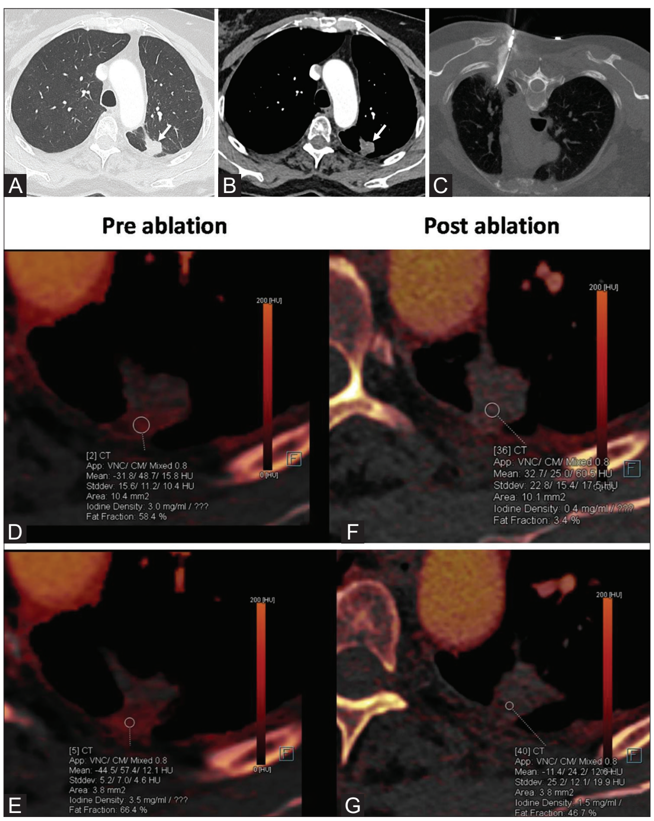

Figure 25 (A-G): Axial HRCT (A) and contrast enhanced (B) images shows an enhancing speculated mass in the left upper lobe (arrows), which on biopsy was proved to be adnocarcinoma. RFA (C) was performed to treat the lesion. The preablation DECT iodine maps (D and E) shows significant iodine uptake, which significantly reduced following RFA (F and G) suggestive of successful ablation

the enhancing masses showing higher values. Our cases also showed similar results [Figures 26 and 27].

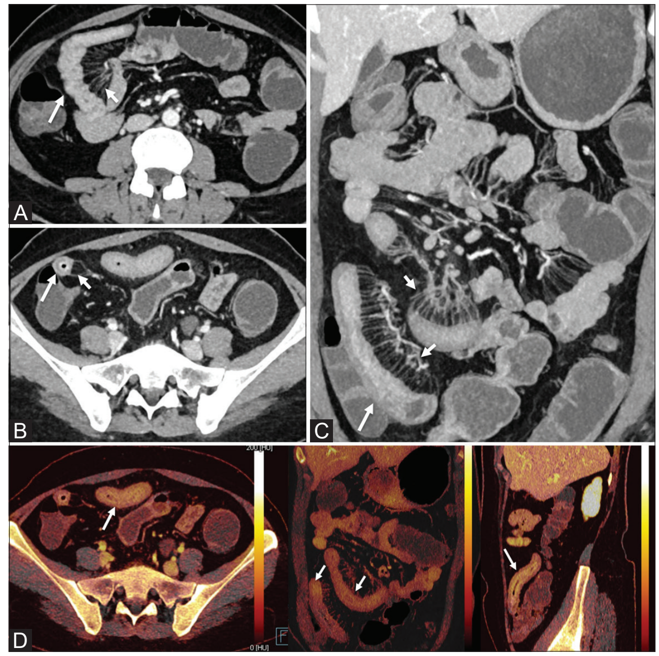

Figure 24 (A-D): 32 years male on treatment for inflammatory bowel disease presented with acute abdominal pain and diarrhoea. The contrast enhanced CT axial (A and B) and coronal (C) images shows multifocal areas of small bowel thickening (arrows) with mesenteric hypervascularity (Comb's sign) (short arrows), fat stranding and lymph nodes, suggestive of inflammatory bowel disease. The DECT iodine maps (D) shows active areas with significant iodine uptake (arrows) in the thickened bowel loops

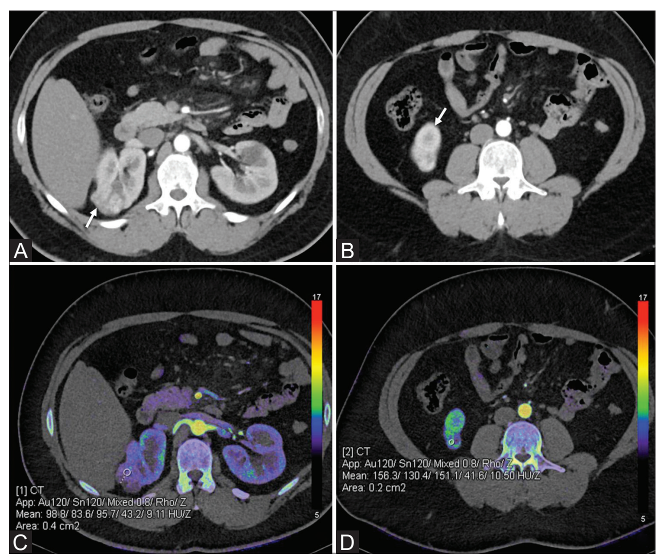

Figure 26 (A-D): The contrast enhanced CT (A and B) images shows 2 enhancing masses (arrows) in the right kidney. The DECT atomic number maps shows Rho/Z values of 9.11 (C) and 10.5 (D) for the two masses, confirming solid enhancing masses

Conclusion

DECT is useful in clinical practice and clearly has many advantages over conventional single energy CT scanners. Various applications described in this pictorial essay highlight the growing importance of DECT. Some new

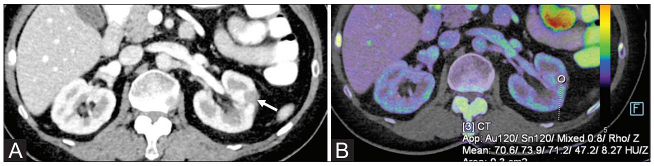

Figure 27 (A and B): The contrast enhanced CT (A) image shows a nonenhancing cystic lesion (arrow) in the left kidney. The DECT atomic number maps shows Rho/Z value of 8.27 (B), confirming non-enhancing cystic lesion

applications which may be used in future are under evaluation. One such example is liver iron estimation in patients with thalassemia.[27,28]

Financial support and sponsorship

Nil.

Conflicts of interest

There are no conflicts of interest.

References

1. Curry TS III, Dowdey JE, Murry RC. Christensen's Physics of Diagnostic Radiology. 4th ed. Philadelphia, PA: Lea and Febiger; 1990. p. 61-9.
2. Alvarez RE, Macovski A. Energy-selective reconstructions in X-ray computerized tomography. Phys Med Biol 1976;21:733-44.
3. Kaza RK, Platt JF, Cohan RH, Caoili EM, Al-Hawary MM, Wasnik A. Dual-energy CT with single- and dual-source scanners: Current applications in evaluating the genitourinary tract. Radiographics 2012;32:353-69.
4. Morhard D, Fink C, Graser A, Reiser MF, Becker C, Johnson TR. Cervical and cranial computed tomographic angiography with automated bone removal: Dual energy computed tomography versus standard computed tomography. Invest Radiol 2009;44:293-7.
5. Sommer WH, Johnson TR, Becker CR, Arnoldi E, Kramer H, Reiser MF, *et al*. The value of dual-energy bone removal in maximum intensity projections of lower extremity computed tomography angiography. Invest Radiol 2009;44:285-92.
6. Pache G, Krauss B, Strohm P, Saueressig U, Blanke P, Bulla S, *et al*. Dual-energy CT virtual noncalcium technique: Detecting posttraumatic bone marrow lesions—feasibility study. Radiology 2010;256:617-24.
7. Guggenberger R, Gnannt R, Hodler J, Krauss B, Wanner GA, Csuka E, *et al*. Diagnostic performance of dual-energy CT for the detection of traumatic bone marrow lesions in the ankle: Comparison with MR imaging. Radiology 2012;264:164-73.
8. Ai S, Qu M, Glazebrook KN, Liu Y, Rhee PC, Leng S, *et al*. Use of dual-energy CT and virtual non-calcium techniques to evaluate post-traumatic bone bruises in knees in the subacute setting. Skeletal Radiol 2014;43:1289-95.
9. Kaup M, Wichmann JL, Scholtz JE, Beeres M, Kromen W, Albrecht MH, *et al*. Dual-energy CT-based display of bone marrow edema in osteoporotic vertebral compression fractures: Impact on diagnostic accuracy of radiologists with varying levels of experience in correlation to MR imaging. Radiology 2016;280:510-9.
10. Brooks RA, Di Chiro G. Beam hardening in X-ray reconstructive tomography. Phys Med Biol 1976;21:390-8.
11. Buck FM, Jost B, Hodler J. Shoulder arthroplasty. Eur Radiol 2008;18:2937-48.
12. Suh JS, Jeong EK, Shin KH, Cho JH, Na JB, Kim DH, *et al*. Minimizing artifacts caused by metallic implants at MR imaging: Experimental and clinical studies. AJR Am J Roentgenol 1998;171:1207-13.
13. Mallinson PI, Coupal TM, McLaughlin PD, Nicolaou S, Munk PL, Ouellette HA. Dual-energy CT for musculoskeletal system. Radiology 2016;281:690-707.
14. Ascenti G, Mazziotti S, Lamberto S, Bottari A, Caloggero S, Racchiusa S, *et al*. Dual-energy CT for detection of endoleaks after endovascular abdominal aneurysm repair: Usefulness of colored iodine overlay. AJR Am J Roentgenol 2011;196:1408-14.
15. Kambadakone AR, Eisner BH, Catalano OA, Sahani DV. New and evolving concepts in the imaging and management of urolithiasis: Urologists' perspective. Radiographics 2010;30:603-23.
16. Pascual E, Batlle-Gualda E, Martínez A, Rosas J, Vela P. Synovial fluid analysis for diagnosis of intercritical gout. Ann Intern Med 1999;131:756-9.
17. Desai MA, Peterson JJ, Garner HW, Kransdorf MJ. Clinical utility of dual-energy CT for evaluation of tophaceous gout. Radiographics 2011;31:1365-75; discussion 76-7.
18. Fink C, Johnson TR, Michaely HJ, Morhard D, Becker C, Reiser M, *et al*. Dual-energy CT angiography of the lung in patients with suspected pulmonary embolism: Initial results. Rofo 2008;180:879-83.
19. Kang MJ, Park CM, Lee CH, Goo JM, Lee HJ. Dual-energy CT: Clinical applications in various pulmonary diseases. Radiographics 2010;30:685-98.
20. Chae EJ, Song JW, Seo JB, Krauss B, Jang YM, Song KS. Clinical utility of dual-energy CT in the evaluation of solitary pulmonary nodules: Initial experience. Radiology 2008;249:671-81.
21. Swensen SJ, Brown LR, Colby TV, Weaver AL. Pulmonary nodules: CT evaluation of enhancement with iodinated contrast material. Radiology 1995;194:393-8.
22. Altenbernd J, Wetter A, Umutlu L, Hahn S, Ringelstein A, Forsting M, *et al*. Dual-energy computed tomography for evaluation of pulmonary nodules with emphasis on metastatic lesions. Actaradiologica 2016;57:437-43.
23. Marin D, Nelson RC, Samei E, Paulson EK, Ho LM, Boll DT, *et al*. Hypervascular liver tumors: Low tube voltage, high tube current multidetector CT during late hepatic arterial phase for detection—initial clinical experience. Radiology 2009;251:771-9.
24. Gupta RT, Ho LM, Marin D, Boll DT, Barnhart HX, Nelson RC. Dual-energy CT for characterization of adrenal nodules: Initial experience. AJR Am J Roentgenol 2010;194:1479-83.
25. Vandenbroucke F, Van Hedent S, Van Gompel G, Buls N, Craggs G, Vandemeulebroucke J, *et al*. Dual-energy CT after radiofrequency ablation of liver, kidney, and lung lesions: A review of features. Insights Imaging 2015;6:363-79.
26. Mileto A, Allen BC, Pietryga JA, Farjat AE, Zarzour JG, Bellini D, *et al*. Characterization of incidental renal mass with dual-energy CT: Diagnostic accuracy of effective atomic number maps for discriminating nonenhancing cysts from enhancing masses. AJR 2017;209:1-10.
27. Luo XF, Xie XQ, Cheng S, Yang Y, Yan J, Zhang H, *et al*. Dual-energy CT for patients suspected of having liver iron overload: Can virtual iron content imaging accurately quantify liver iron content? Radiology 2015;277:95-103.
28. Joe E, Kim SH, Lee KB, Jang JJ, Lee JY, Lee JM, *et al*. Feasibility and accuracy of dual-source dual-energy CT for noninvasive determination of hepatic iron accumulation. Radiology 2012;262:126-35.